Biointerface Research in Applied Chemistry
Open-Access Journal (ISSN: 2069-5837)

Article
Volume 16, Issue 1, 2026, 29
https://doi.org/10.33263/BRIAC161.029

DynamicBind and Molecular Dynamics Study of Diarylheptanoids from *Curcuma comosa* Roxb. as Potential Caspase-3 Inhibitors

Prasan Tangyuenyongwatana [1,*]

[1] Department of Pharmaceutical Industry, School of Pharmacy, Eastern Asia University, Pathum Thani, 12000, Thailand
* Correspondence: prasan@eau.ac.th;

Received: 19.07.2025; Accepted: 18.12.2025; Published: 15.02.2026

Abstract: The discovery of caspase-3 inhibitors is a significant area in drug development. Diarylheptanoids from *Curcuma comosa* rhizomes present a promising source of such inhibitors. This study explores the use of DynamicBind, a deep learning-based docking program, as a tool for identifying potential inhibitors. The optimal parameters for DynamicBind docking, including the number of samples, inference steps, and seed number, were validated. The accuracy was tested by redocking an X-ray ligand into caspase-3 (1NMS), achieving an RMSD of 0.536 Å. Six diarylheptanoids were docked, and compound 3 showed a low RMSD (0.827 Å) and a strong confidence score (cLDDT 0.625), interacting with four amino acids in the binding site, matching those in the X-ray ligand of 1NMS. Notably, GLY122 was unique to this test and may be key to its activity. These results are consistent with the reported anti-apoptotic activity. Molecular dynamics simulations with GROMACS confirm the binding results and reveal the complex's stability. In conclusion, DynamicBind is an evolved docking program for identifying protein-ligand pairs without prior knowledge of the binding site. It can isolate an active compound from inactive derivatives with greater confidentiality. This program has potential prominence in drug design and discovery.

Keywords: DynamicBind; caspase-3 inhibitors; diarylheptanoids; molecular dynamics; deep learning-based approach.

© 2026 by the authors. This article is an open-access article distributed under the terms and conditions of the Creative Commons Attribution (CC BY) license (https://creativecommons.org/licenses/by/4.0/), which permits unrestricted use, distribution, and reproduction in any medium, provided the original work is properly cited. The authors retain copyright of their work, and no permission is required from the authors or the publisher to reuse or distribute this article, as long as proper attribution is given to the original source.

1. Introduction

Molecular docking has long been an important tool in computer-aided drug design to predict the binding of small molecules to proteins [1]. Conventional software such as AutoDock 4, AutoDock Vina [2], GOLD [3,4], Glide [5,6], and SwissDock [7] often treat proteins as rigid, static structures. Recently, powerful GPUs have been utilized to accelerate molecular docking. Comprehensive evaluations showed that the GPU implementation surpasses the CPU method in both execution speed and docking accuracy [8]. In addition, static docking has limitations because proteins are dynamic and could change conformation upon ligand binding. To address this limitation, dynamic docking uses multiple protein structures from simulations or experiments to predict better binding poses, especially for flexible proteins [9]. More recently, AI-based methods like DeepDock [10], EquiBind [11], DiffDock [12], and CarsiDock [13] have improved accuracy by learning from large datasets and recognizing complex patterns that traditional methods may have missed.

DynamicBind, introduced by Lu *et al*., is a geometric deep generative model that represents a major advance in molecular docking by directly modeling protein flexibility during ligand binding [14]. Unlike traditional rigid docking approaches, DynamicBind performs "dynamic docking," efficiently adjusting protein conformations from an initial (apo-like) structure to a ligand-bound (holo-like) state. The process begins with an unbound protein and a small-molecule ligand, generating initial ligand positions stochastically. Docking proceeds through 20 iterative cycles: in the first five, only the ligand's position and conformation are refined, while the protein remains static; in subsequent cycles, both ligand and protein undergo coordinated adjustments, including translation, rotation, and side-chain angle refinement, to capture realistic binding-induced conformational changes. At each stage, an SE(3)-equivariant graph neural network processes the three-dimensional features of the protein-ligand system, ensuring predictions respect spatial symmetries and enabling efficient sampling of large conformational changes [15–17]. DynamicBind employs a morph-like transformation. This approach allows DynamicBind to generate multiple plausible protein-ligand complex structures [18]. It can unify protein conformation generation and ligand pose prediction, perform global docking, and identify cryptic pockets.

DynamicBind differs from EquiBind and DiffDock in several ways. First, DynamicBind models both ligand and protein flexibility during docking. In contrast to protein flexibility, DiffDock and EquiBind treat the protein as rigid, adjusting only the ligand pose. Equibind represents protein structures as graphs, and their atomic positions do not change during docking. DiffDock treats the protein backbone as static/rigid during docking, but it allows limited protein flexibility through side-chain adjustments. The next part, DynamicBind, uses a morph-like transformation, while EquiBind uses regression to directly predict a single average binding pose, potentially missing multiple or physically realistic poses [12]. DiffDock applies a diffusion process [13]. Benchmarks show that DynamicBind matches or outperforms existing methods in docking accuracy and virtual screening, especially for proteins whose shapes change significantly upon ligand binding [19].

Caspase-3 is a member of the cysteine-aspartic acid protease (caspase) family, which is widely recognized as the executioner in the apoptotic pathway [20]. The active site of caspase-3 features a catalytic dyad consisting of Cys-163 and His-121. A hydrophobic patch on the protein surface consists of amino acid residues Tyr-204, Trp-206, and Phe-250. In 2008, Suksamrarn *et al*. isolated 12 diarylheptanoids from *Curcuma comosa* Roxb. rhizomes and evaluated their potential pharmacological activities [21]. In 2016, Vattanarongkup *et al*. found that only one compound from this herb influences anti-apoptotic activity and affects caspase-3 protein expression [22].

Based on the information presented above, this study was designed with four specific objectives. First, to validate the docking variables—number of samples, inference steps, and seed number—to determine the optimal conditions for DynamicBind docking. Second, to assess its accuracy by redocking the X-ray ligand of the caspase-3 protein. Third, to use DynamicBind to dock six diarylheptanoids, selected from 12 compounds from *Curcuma comosa* Roxb., for their minor structural differences and diverse functional groups, in order to assess their anti-apoptotic activity with the flexible target protein. Finally, select the best-performing compounds from the docking studies and conduct molecular dynamics simulations with GROMACS to observe the stability of these complexes. These processes should demonstrate the outstanding ability of the new deep learning and neural network docking program to predict anti-apoptosis activity.

2. Materials and Methods

2.1. Target for docking screening.

Caspase-3 (PDB ID: 1NMS) was selected from the Protein Data Bank (www.rcsb.org) and screened with PDBFIXER (https://anaconda.org/conda-forge/pdbfixer/, https://neurosnap.ai/) to fill gaps in the protein sequence where residues are missing in the crystal structure. The fixed protein was then submitted to the DynamicBind 2.0 program on the Neurosnap web platform (https://neurosnap.ai/).

2.2. Compound selection for docking study.

Six compounds were selected from *Curcuma comosa* Roxb. rhizomes, as reported by Suksamrarn *et al*., and the structures are shown in Figure 1 [21]. Next, the structures of these compounds were obtained from PubChem (https://pubchem.ncbi.nlm.nih.gov/) as SDF files. They were then subjected to performing docking with the DynamicBind 2.0 program. In this experiment, the reference compound was 4-[(E,3S)-3-hydroxy-7-phenylhept-6-enyl]benzene-1,2-diol.

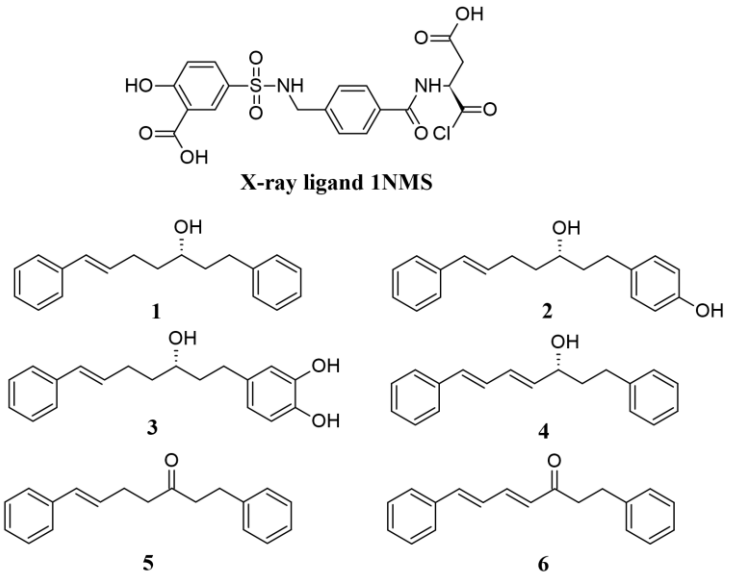

Figure 1. Structures of X-ray ligand of 1NMS and diaryheptanoids from *Curcuma comosa* Roxb. rhizomes.

2.3. Docking parameters of DynamicBind.

2.3.1. Validation of docking parameters.

Three key parameters can be configured to optimize the DynamicBind docking process: the number of samples, the number of inference steps, and a seed value from a random table. Validated experiments systematically varied inference steps (10, 20, 30, 40, 50) and the number of generated samples (10, 20, 30, 40, 50) while keeping the seed fixed at 42. For seed variation, 10 randomly assigned seeds were used, with a fixed sample size and inference steps. The 10 seed numbers were 7, 16, 33, 84, 234, 566, 891, 1112, 2024, and 5055. Each run's pose structures were checked against the reference compound, and RMSD was calculated using PyMOL 2.1 (Schrödinger, USA). Average RMSDs plus standard deviations were graphed against sample number and each inference step using GraphPad Prism 10 (GraphPad, USA).

By default, the system predicts results and ranks 10–50 poses. For example, if 10 are chosen, rank 1 is the best and rank 10 is the lowest. The number of inference steps (10–50)

controls how many coordinate updates the model makes, balancing accuracy and speed; more steps (e.g., 50) improve exploration but take longer. After prediction, a relaxation step is included in the process and recommended to refine and enhance the protein-ligand structure. Setting a random seed (1–100 or higher) makes results reproducible—using the same seed and input will give the same result. If no seed is set (seed = 0), the program picks one randomly, and results may vary unless the seed is recorded.

2.3.2. Redock for accuracy evaluation.

The dynamicBind redock test used the best condition from the validation process, and the redock was repeated 3 times (n = 3). Additionally, the PyRx 0.8 program was used as a reference in blind docking mode. The binding site coordinates (X = 5.4416, Y = 3.7977, Z = 19.4307) and box dimensions (X = 68.4318, Y = 60.1418, Z = 47.5506) were set to cover the whole protein. The exhaustiveness level was set to 8. The redock was also repeated 3 times (n = 3).

2.3.3. Docking with test compounds.

After obtaining the appropriate sample numbers and inference steps, the two best optimal seed numbers were selected. These parameters were applied to the six *C. comosa* test compounds. After docking six compounds, the core structures of each docked pose were superimposed onto the reference structure using PyMOL 2.1 and VEGA ZZ. For ligand-protein interactions, the Discovery Studio Visualizer program (Dassault Systèmes, France) was used. DynamicBind also evaluates predicted protein-ligand complex structures using contact-LDDT (cLDDT), a metric adapted from the local Distance Difference Test in AlphaFold [23], which measures geometric and physicochemical compatibility, as well as structural stability and accuracy. DynamicBind ranks poses to identify the most structurally plausible binding conformations.

2.4. Molecular dynamics study.

Molecular dynamics simulations were performed using GROMACS to assess the stability of the caspase-3 protein (1NMS) complex from DynamicBind docking and the 1NMS ligand-protein complex for comparison. Simulations used the AMBER99SB-ILDN force field, a dodecahedron TIP3P water box, Na^+ and Cl^- ions (0.15 M), and energy minimization via the steepest descent algorithm. Equilibration included NVT (300 K, 100 ps, velocity-rescale) and NPT (1 bar, 100 ps, Berendsen). The production run (10 ns, NPT, Parrinello-Rahman, 2-fs time step) used LINCS constraints and the Verlet scheme. Trajectories were saved every 10 ps. Analyses included RMSD, RMSF, and radius of gyration. The Root Mean Square Deviation (RMSD) was calculated for the backbone and C-alpha (Cα) atoms by aligning each frame of the trajectory to the initial energy-minimized structure. The simulation error was estimated from the fluctuations during the equilibrated phase of the trajectory (2,000-10,000 ps).

3. Results and Discussion

3.1. Docking results on parameter validation.

A validation study was conducted using DynamicBind to identify the optimal parameters for the experimental docking protocol under the specified conditions. The number

of inference steps (10, 20, 30, 40, 50) and the number of samples generated (10, 20, 30, 40, 50) were systematically varied with three runs on each condition (n = 3), with the seed fixed at 42. The accuracy of each parameter set was checked. This included evaluating the number of selected poses, and the RMSD was measured relative to the reference compound. The RMSD (mean ± SD) values are displayed in Figure 2.

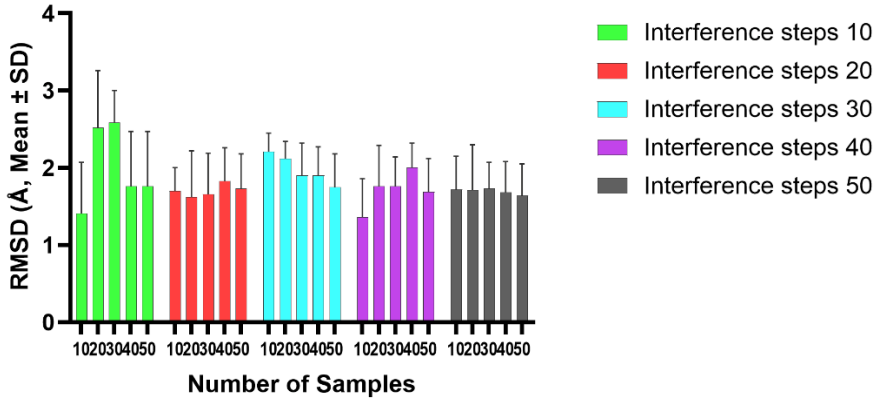

Figure 2. DynamicBind docking results with variation on the number of samples (10-50) and the number of inference steps (10-50). The number of samples is 10, and the number of inferences is 40, giving the optimal RMSD values.

The experimental results shown in Figure 3 indicate that the number of inference steps crucially affects docking accuracy. The most accurate prediction was obtained with 40 inference steps and 10 samples, yielding the lowest mean RMSD of 1.32 ± 0.32 Å. Additionally, both 20 and 50 inference steps delivered consistent and robust performance, yielding RMSD values typically between 1.6 Å and 1.8 Å, regardless of sample size. All values remain well below the 2.0 Å threshold for docking success.

This validation used a single random seed. Some parameter sets performed poorly, and results varied. For example, with 10 inference steps, ten samples produced a good pose, but 20 or 30 samples led to worse outcomes, with RMSD values above 2.5 Å. Increasing to 40 inference steps also raised the mean RMSD, often near the 2.0 Å cutoff. This shows that an optimal balance exists between inference steps and accuracy. In methods like DynamicBind, the seed influences the search path and the decisions made, so performance can depend on the chosen path. For instance, the strong result with 40 inference steps and 10 samples might be due to chance, while poor outcomes elsewhere could reflect unlucky paths. To confirm reliability and rule out random chance, a multi-seed study would be conducted.

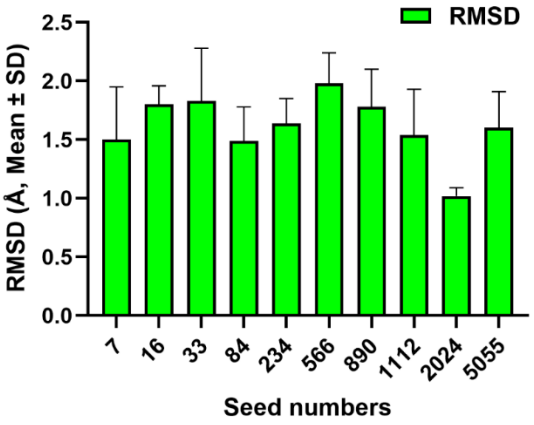

Figure 3. RMSD values for DynamicBind docking with varying seed numbers. Error bars represent the 95% confidence interval (n=10).

Figure 3 shows that running the docking algorithm with different random seeds highlights its stochastic nature. Using multiple seeds helps sample conformational space and tests the consistency of finding the correct solution. To ensure results were not dependent on the initial seed, each experiment was repeated 10 times with independent, randomly chosen seeds. All runs converged to the correct binding pose; the mean RMSD across 10 random seeds was 1.60 Å, indicating RMSD values consistently below 2.0 Å and demonstrating the robustness of the predicted binding mode. Seeds were categorized as "good," "medium," or "poor" based on RMSD values. Seed 2024 performed with the best RMSD of 1.02 Å. Seeds 7, 84, and 1112 were considered medium with RMSD below 1.54 Å. The rest had RMSD values from 1.60 to 1.98 Å. Note that these seeds were specific to this system; new seeds should be tested for different proteins or ligands.

3.2. Redock.

To evaluate docking accuracy, DynamicBind redocked the X-ray ligand into its native protein (PDB ID: 1NMS) under two satisfactory conditions. Specifically, the first condition was number of samples = 10, inference steps = 40, and seed number = 2024. The second condition was number of samples = 10, inference steps = 20, and seed number = 84. Both DynamicBind and the standard docking program, PyRx 0.8, show redocked poses in Figure 4. The RMSD results are summarized in Figure 5. For DynamicBind, two seed numbers were tested. A seed of 2024 yielded an RMSD of 0.716 ± 0.048 Å (cLDDT = 0.634, n=3), while a seed of 84 produced a more accurate pose with a lower RMSD of 0.536 ± 0.019 Å and a higher confidence score (cLDDT = 0.654, n=3). As a benchmark, a blind redocking was performed with PyRx. At the default exhaustiveness setting of 8, the RMSD was significantly higher at 0.971 ± 3.73 Å. Increasing the exhaustiveness to 16 did not improve the result, further increasing the RMSD to 1.525 ± 0.307 Å. The binding energies for PyRx were -7.86 ± 0.23 kcal/mol (for exh. 8) and -7.80 ± 0.17 kcal/mol (for exh. 16). DynamicBind consistently produced a more accurate docking pose with a lower RMSD than PyRx. While all tested methods yielded RMSDs below the 2.0 Å threshold for successful docking, DynamicBind's superior performance and conformational accuracy make it the more reliable approach for this system.

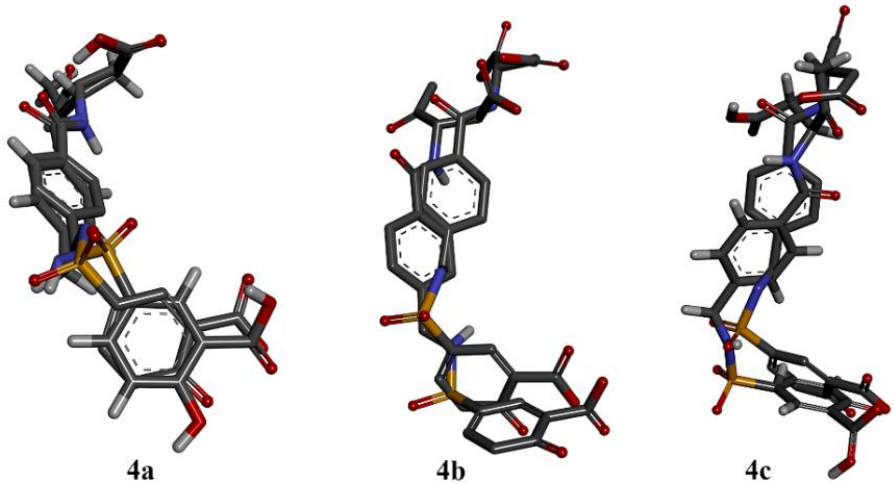

Figure 4. Redock X-ray ligand overlay with parent ligand of protein 1NMS **(a)** by the DynamicBind program; **(b)** by PyRx 0.8 at exhaustiveness = 8; **(c)** at exhaustiveness = 16. The DynamicBind pose shows a good overlay of the structure over PyRx 0.8 docking poses at both exhaustiveness values.

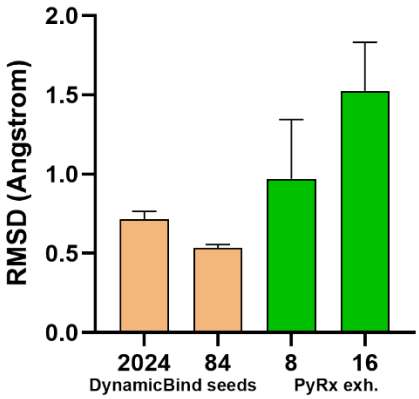

Figure 5. The RMSD of DynamicBind and PyRx redocking values, with DynamicBind showing better results. Error bars represent the standard deviation (n=3).

3.3. Docking with test compounds.

The test compounds 1–6 were docked into protein 1NMS with the seed number 84 condition. The docking results are presented in Figure 6. The cLDDT score for each pose reflects the stability of the protein structure in that specific pose. Compound 3 exhibited the lowest RMSD of 0.827 Å and a high cLDDT confidence score (0.625), and interactions with the required amino acids in the heatmap below. All these components indicate that the protein-ligand structure is more stable than that of other test compounds. If the cLDDT score is low for a particular pose, it suggests that the protein complex is less stable or has deviated significantly from its reference conformation, as shown in Figure 7.

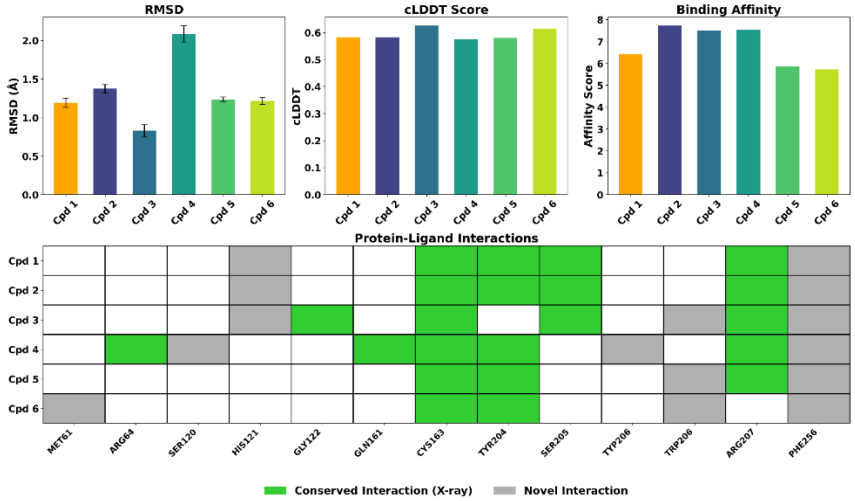

Figure 6. Docking results for the DynamicBind program for compounds 1–6 are presented, including RMSD (n = 3), cLDDT scores, and binding affinity. The heatmap below shows protein–ligand interactions compared to the X-ray ligand (1NMS).

A detailed analysis of the ligand-protein interactions shows that active compound 3 forms several key binding site contacts, consistent with the reference ligand (Figure 8). These include interactions with CYS163, SER205, and ARG207. Notably, compound 3 uniquely interacts with GLY122. It forms conventional hydrogen bonds between its phenyl hydroxy group and both CYS163 and GLY122. The X-ray ligand of 1NMS also interacts with these amino acids. This GLY122 interaction is absent in all other tested compounds and is hypothesized to be essential for the observed inhibitory activity. The other compounds showed lower cLDDT scores and weaker Pi-hydrogen interaction between their phenyl group and

CYS163. Most compounds have the phenyl group on one or both sides bumping into the binding site at CYS163, TYR204, TRP206, and PHE256.

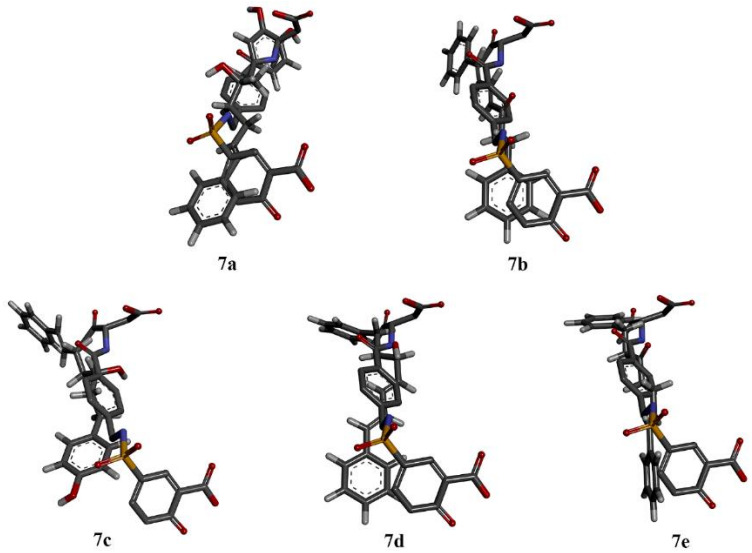

Figure 7. Compounds overlay with 1NMS X-ray ligand: **(a)** compound 3; **(b)** compound 6; **(c)** compound 2; **(d)** compound 4; **(e)** compound 5. All compound poses show that DynamicBind can find the binding site, similar to blind docking but more precise.

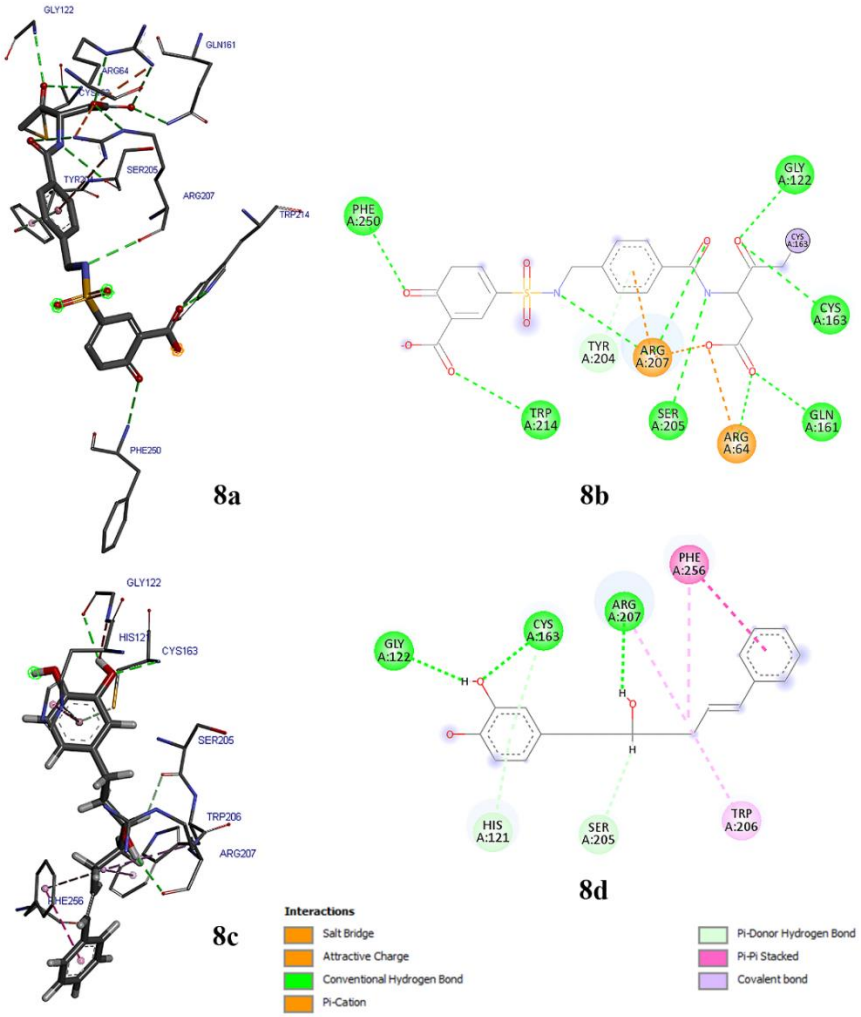

Figure 8. Protein 1NMS interacts with ligands. **(a)** The 3D X-ray ligand of 1NMS interacts with amino acids in the binding site; **(b)** 2D map of the X-ray ligand of 1NMS interacting with amino acids; **(c)** Compound 3 interacts with amino acids in the binding site; **(d)** 2D map of compound 3 interacting with the amino acids of the 1NMS protein.

3.3. Molecular dynamics study.

3.3.1. Trajectory comparison and RMSD analysis of the two complexes.

In DynamicBind, the complex of compound 3 with the caspase-3 protein (1NMS) showed high cLDDT and low RMSD. This complex was subjected to binding stability testing using GROMACS. The results were compared with those of the X-ray ligand in the 1NMS complex. The trajectory and RMSD of two complexes are shown in Figure 9.

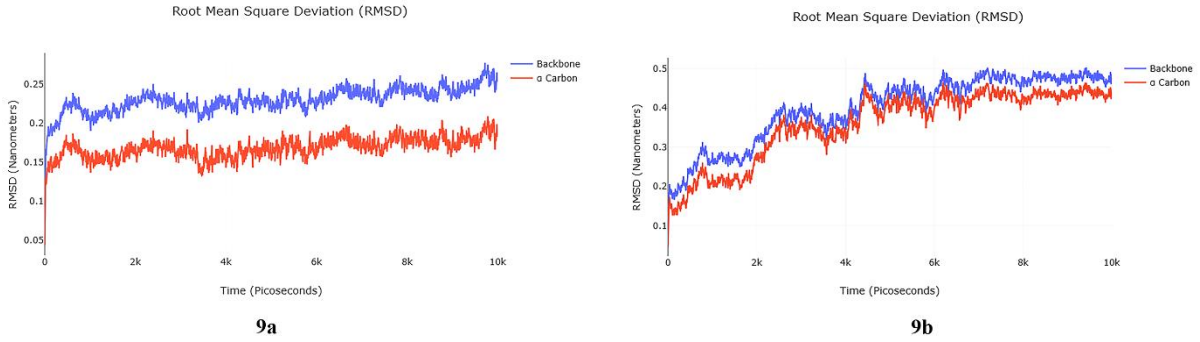

Figure 9. (a) The molecular dynamics trajectory of compound 3 shows rapid stabilization with low fluctuation; **(b)** the X-ray ligand in 1NMS shows greater fluctuation at the early stage and becomes more stable in the latter period.

The molecular dynamics trajectories of compound 3 and the X-ray ligand for 1NMS show apparent differences. Compound 3 stabilizes rapidly with minimal fluctuations, likely due to its simpler structure and fewer functional groups, allowing efficient binding. When examining observations from the trajectory plots of compound 3 in Figure 9a, the RMSD for the backbone stabilizes around 0.2–0.25 nm after approximately 2 ns and remains relatively stable throughout the simulation. The RMSD for the alpha carbons stabilizes around 0.15–0.2 nm, with only minor fluctuations, suggesting that the protein-ligand complex is relatively stable. In contrast, the X-ray ligand fluctuates more and takes longer to stabilize, probably because its larger size and greater number of functional groups create initial instability and more potential interactions. For 1NMS with the X-ray ligand in Figure 9b, the backbone RMSD stabilizes around 0.4–0.5 nm after approximately 4 ns, with some fluctuations, and the RMSD for the alpha carbons also stabilizes around 0.35–0.45 nm with similar fluctuations. These larger fluctuations indicate that the protein-ligand complex is less stable compared to the compound 3 system.

3.3.2. Comparing the RMSF of the two complexes.

Root-mean-square fluctuation (RMSF) plots show the flexibility of individual residues during molecular dynamics (MD) simulations. For 1NMS with the X-ray ligand (Figure 10a), RMSF values are generally low (~0.1–0.2 nm) for most residues, indicating a stable protein structure. However, a high peak around residues 143–150 (ASP143, MET145, ALA146, CYS147, HIS148, LYS149, and ISO150 (Figure 11) indicates localized flexibility arising from terminal residues or flexible side chains. For 1NMS with compound 3 (Figure 10b), RMSF values are lower (~0.05–0.15 nm), indicating a more stable protein structure than the previous one. The peaks are less pronounced, showing no extreme fluctuations. Residues in contact with compound 3 appear more stable, suggesting fewer steric clashes and better complementarity with the binding pocket.

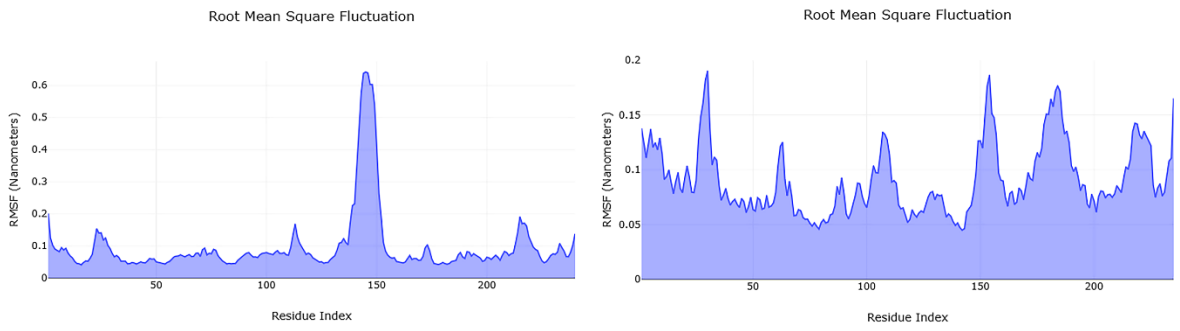

10a **10b**

Figure 10. The RMSF of the X-ray **(a)** ligand shows a high peak around residues 143–150, while **(b)** compound 3 shows low fluctuation of the dynamic complex.

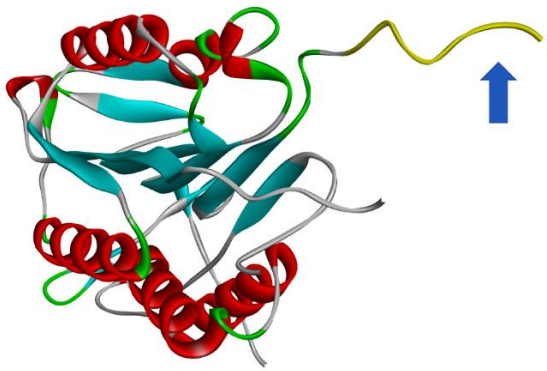

Figure 11. The segment of the amino acid residue index from 143 to 150, indicated by an arrow pointing to the yellow part, indicates localized flexibility.

All molecular dynamics parameter results for compounds 1-6 are summarized in Figure 12. The RMSD, RMSF, and radius of gyration plots for compounds 1-6 are shown in Supplementary Materials, Figures S1-S6, respectively.

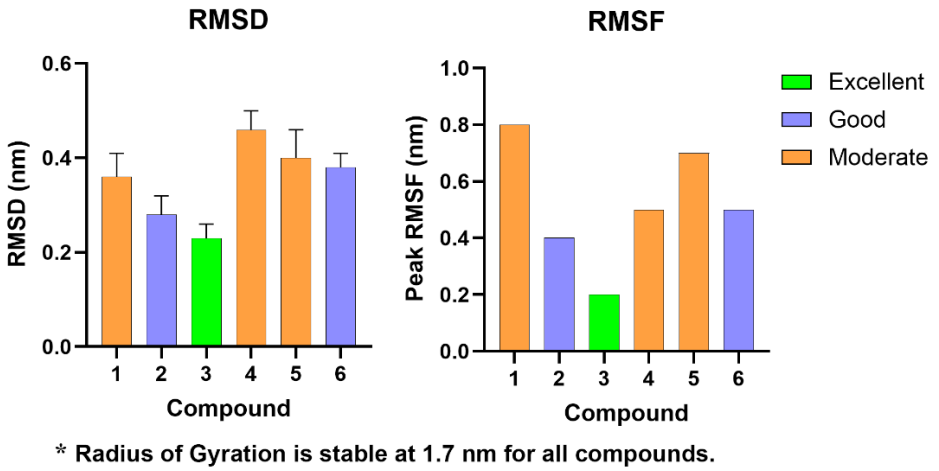

Figure 12. Summarized MD simulation metrics for compounds 1-6. Compound 3 shows the lowest RMSD and RMSF among the derivatives.

In Figure 12, compound 3 shows the most stable binding, with the lowest RMSD and RMSF, while the other derivatives, which differ only slightly in structure, have higher values for both parameters. Compound 3 is the only compound known to have biological activity that provides cytoprotective effects on C6 astroglial cells under oxidative stress from hydrogen peroxide (H_2O_2). It protects against H_2O_2-induced apoptosis. This occurs by inhibiting increases in cleaved caspase-3, phosphorylated p53, and the Bax/Bcl-2 ratio, as reported by

Vattanarongkup and coworkers. Khin Aung *et al*. also found that compound 3 reduces apoptotic cell death by lowering cleaved caspase-3 and phospho-p53 expression [24]. No other diaryheptanoids in this herb have been reported to have this activity.

4. Conclusions

The results show that the DynamicBind achieves highly accurate redocking of the x-ray ligand into the 1NMS protein. It surpasses the traditional PyRx 0.8 program in both default and increased exhaustiveness settings. Crucially, DynamicBind successfully distinguished the known biologically active compound (compound 3) from its inactive derivatives, predicting a superior binding pose and confidence score. These results highlight DynamicBind's superior accuracy and reliability in docking studies without prior knowledge of the binding site. The molecular dynamics simulations confirm that compound 3 forms a stable, complementary interaction with the target protein. DynamicBind marks an evolution in docking programs by using deep learning and neural networks to identify protein-ligand pairs. This represents a significant advancement for docking methodology, distinct from conventional molecular mechanics docking and some AI docking programs. This new approach offers significant potential as a tool for future drug discovery. For future work, DynamicBind will be used to study how ligand binding at a specific allosteric site affects activity at another site.

Author Contributions

Conceptualization, P.T.; methodology, P.T.; software, P.T.; validation, P.T.; formal analysis, P.T.; investigation, P.T.; resources, P.T.; data curation, P.T.; writing—original draft preparation, P.T.; writing—review and editing, P.T.; visualization, P.T.; supervision, P.T.; project administration, P.T. All authors have read and agreed to the published version of the manuscript.

Institutional Review Board Statement

Not applicable.

Informed Consent Statement

Not applicable.

Data Availability Statement

Data supporting the findings of this study are available upon reasonable request from the corresponding author.

Funding

This research received no external funding.

Acknowledgments

The author would like to thank the School of Pharmacy at Eastern Asia University for their contributions, including administrative and technical support for computing devices. The author also extends sincere gratitude to Athiwat Hutchaleelaha, Ph.D., of BridgeBio, San

Francisco, CA, USA, for his thoughtful review and helpful language refinement on this manuscript.

Conflicts of Interest

The author declares no conflict of interest.

References

1. Agu, P.C.; Afiukwa, C.A.; Orji, O.U.; Ezeh, E.M.; Ofoke, I.H.; Ogbu, C.O.; Ugwuja, E.I.; Aja, P.M. Molecular docking as a tool for the discovery of molecular targets of nutraceuticals in diseases management. *Sci. Rep.* **2023**, *13*, 13398, https://doi.org/10.1038/s41598-023-40160-2.
2. Trott, O.; Olson, A.J. AutoDock Vina: Improving the speed and accuracy of docking with a new scoring function, efficient optimization, and multithreading. *J. Comput. Chem.* **2010**, *31*, 455–461, https://doi.org/10.1002/jcc.21334.
3. Jones, G.; Willett, P.; Glen, R.C.; Leach, A.R.; Taylor, R. Development and validation of a genetic algorithm for flexible docking. *J. Mol. Biol.* **1997**, *267*, 727–748, https://doi.org/10.1006/jmbi.1996.0897.
4. David, L.; Mdahoma, A.; Singh, N.; Buchoux, S.; Pihan, E.; Diaz, C.; Rabal, O. A toolkit for covalent docking with GOLD: from automated ligand preparation with KNIME to bound protein–ligand complexes. *Bioinform. Adv.* **2022**, *2*, vbac090, https://doi.org/10.1093/bioadv/vbac090.
5. Friesner, R.A.; Banks, J.L.; Murphy, R.B.; Halgren, T.A.; Klicic, J.J.; Mainz, D.T.; Repasky, M.P.; Knoll, E.H.; Shelley, M.; Perry, J.K.; Shaw, D.E.; Francis, P.; Shenkin, P.S. Glide: A New Approach for Rapid, Accurate Docking and Scoring. 1. Method and Assessment of Docking Accuracy. *J. Med. Chem.* **2004**, *47*, 1739-1749, https://doi.org/10.1021/jm0306430.
6. Shamsian, S.; Sokouti, B.; Dastmalchi, S. Benchmarking different docking protocols for predicting the binding poses of ligands complexed with cyclooxygenase enzymes and screening chemical libraries. *BioImpacts* **2023**, *14*, 29955, https://doi.org/10.34172/bi.2023.29955.
7. Bugnon, M.; Röhrig, U.F.; Goullieux, M.; Perez, M.A.S.; Daina, A.; Michielin, O.; Zoete, V. SwissDock 2024: major enhancements for small-molecule docking with Attracting Cavities and AutoDock Vina. *Nucleic Acids Res.* **2024**, *52*, W324-W332, https://doi.org/10.1093/nar/gkae300.
8. Fan, M.; Wang, J.; Jiang, H.; Feng, Y.; Mahdavi, M.; Madduri, K.; Kandemir, M.T.; Dokholyan, N.V. GPU-Accelerated Flexible Molecular Docking. *J. Phys. Chem. B* **2021**, *125*, 1049-1060, https://doi.org/10.1021/acs.jpcb.0c09051.
9. Amaro, R.E.; Baudry, J.; Chodera, J.; Demir, Ö.; McCammon, J.A.; Miao, Y.; Smith, J.C. Ensemble Docking in Drug Discovery. *Biophys. J.* **2018**, *114*, 2271-2278, https://doi.org/10.1016/j.bpj.2018.02.038.
10. Gentile, F.; Agrawal, V.; Hsing, M.; Ton, A.-T.; Ban, F.; Norinder, U.; Gleave, M.E.; Cherkasov, A. Deep Docking: A Deep Learning Platform for Augmentation of Structure Based Drug Discovery. *ACS Cent. Sci.* **2020**, *6*, 939-949, https://doi.org/10.1021/acscentsci.0c00229.
11. Li, Y.; Li, L.; Wang, S.; Tang, X. EQUIBIND: A geometric deep learning-based protein-ligand binding prediction method. *Drug Discov. Ther.* **2023**, *17*, 363-364, https://doi.org/10.5582/ddt.2023.01063.
12. Corso, G.; Stärk, H.; Jing, B.; Barzilay, R.; Jaakkola, T. Diffdock: Diffusion steps, twists, and turns for molecular docking. *arXiv preprint arXiv:2210.01776* **2022**, https://doi.org/10.48550/arXiv.2210.01776.
13. Cai, H.; Shen, C.; Jian, T.; Zhang, X.; Chen, T.; Han, X.; Yang, Z.; Dang, W.; Hsieh, C.-Y.; Kang, Y.; Pan, P.; Ji, X.; Song, J.; Hou, T.; Deng, Y. CarsiDock: a deep learning paradigm for accurate protein–ligand docking and screening based on large-scale pre-training. *Chem. Sci.* **2024**, *15*, 1449-1471, https://doi.org/10.1039/d3sc05552c.
14. Lu, W.; Zhang, J.; Huang, W.; Zhang, Z.; Jia, X.; Wang, Z.; Shi, L.; Li, C.; Wolynes, P.G.; Zheng, S. DynamicBind: predicting ligand-specific protein-ligand complex structure with a deep equivariant generative model. *Nat. Commun.* **2024**, *15*, 1071, https://doi.org/10.1038/s41467-024-45461-2.
15. Batzner, S.; Musaelian, A.; Sun, L.; Geiger, M.; Mailoa, J.P.; Kornbluth, M.; Molinari, N.; Smidt, T.E.; Kozinsky, B. E(3)-equivariant graph neural networks for data-efficient and accurate interatomic potentials. *Nat. Commun.* **2022**, *13*, 2453, https://doi.org/10.1038/s41467-022-29939-5.
16. Gupta, A.K.; Stulajter, M.M.; Shaidu, Y.; Neaton, J.B.; de Jong, W.A. Equivariant Neural Networks Utilizing Molecular Clusters for Accurate Molecular Crystal Lattice Energy Predictions. *ACS Omega* **2024**, *9*, 40269-40282, https://doi.org/10.1021/acsomega.4c07434.

17. Roche, R.; Moussad, B.; Shuvo, M.H.; Bhattacharya, D. E(3) equivariant graph neural networks for robust and accurate protein-protein interaction site prediction. *PLoS Comput. Biol.* **2023**, *19*, e1011435, https://doi.org/10.1371/journal.pcbi.1011435.
18. Lee, B.H.; Park, S.W.; Jo, S.; Kim, M.K. Protein conformational transitions explored by a morphing approach based on normal mode analysis in internal coordinates. *PLOS ONE* **2021**, *16*, e0258818, https://doi.org/10.1371/journal.pone.0258818.
19. Lee, J.; Hao Nguyen, C.; Mamitsuka, H. Beyond rigid docking: deep learning approaches for fully flexible protein–ligand interactions. *Brief. Bioinform.* **2025**, *26*, bbaf454, https://doi.org/10.1093/bib/bbaf454.
20. Aziz, U.; Nigel, H.G.; Mohammad Amjad, K. Inhibition of Caspase 3 and Caspase 9 Mediated Apoptosis: A Multimodal Therapeutic Target in Traumatic Brain Injury. *Curr. Neuropharmacol.* **2023**, *21*, 1001-1012, https://doi.org/10.2174/1570159X20666220327222921.
21. Suksamrarn, A.; Ponglikitmongkol, M.; Wongkrajang, K.; Chindaduang, A.; Kittidanairak, S.; Jankam, A.; Yingyongnarongkul, B.-e.; Kittipanumat, N.; Chokchaisiri, R.; Khetkam, P.; Piyachaturawat, P. Diarylheptanoids, new phytoestrogens from the rhizomes of *Curcuma comosa*: Isolation, chemical modification and estrogenic activity evaluation. *Bioorg. Med. Chem.* **2008**, *16*, 6891-6902, https://doi.org/10.1016/j.bmc.2008.05.051.
22. Vattanarongkup, J.; Piyachaturawat, P.; Tuchinda, P.; Sanvarinda, P.; Sanvarinda, Y.; Jantaratnotai, N. Protective effects of a diarylheptanoid from *Curcuma comosa* against hydrogen peroxide-induced astroglial cell death. *Planta Med.* **2016**, *82*, 1456-1462, https://doi.org/10.1055/s-0042-109173.
23. Jumper, J.; Evans, R.; Pritzel, A.; Green, T.; Figurnov, M.; Ronneberger, O.; Tunyasuvunakool, K.; Bates, R.; Žídek, A.; Potapenko, A.; Bridgland, A.; Meyer, C.; Kohl, S.A.A.; Ballard, A.J.; Cowie, A.; Romera-Paredes, B.; Nikolov, S.; Jain, R.; Adler, J.; Back, T.; Petersen, S.; Reiman, D.; Clancy, E.; Zielinski, M.; Steinegger, M.; Pacholska, M.; Berghammer, T.; Bodenstein, S.; Silver, D.; Vinyals, O.; Senior, A.W.; Kavukcuoglu, K.; Kohli, P.; Hassabis, D. Highly accurate protein structure prediction with AlphaFold. *Nature* **2021**, *596*, 583-589, https://doi.org/10.1038/s41586-021-03819-2.
24. Khin Aung, Z.M.; Jantaratnotai, N.; Piyachaturawat, P.; Sanvarinda, P. A pure compound from *Curcuma comosa* Roxb. protects neurons against hydrogen peroxide-induced neurotoxicity via the activation of Nrf-2. *Heliyon* **2022**, *8*, e11228, https://doi.org/10.1016/j.heliyon.2022.e11228.

Publisher's Note & Disclaimer

The statements, opinions, and data presented in this publication are solely those of the individual author(s) and contributor(s) and do not necessarily reflect the views of the publisher and/or the editor(s). The publisher and/or the editor(s) disclaim any responsibility for the accuracy, completeness, or reliability of the content. Neither the publisher nor the editor(s) assume any legal liability for any errors, omissions, or consequences arising from the use of the information presented in this publication. Furthermore, the publisher and/or the editor(s) disclaim any liability for any injury, damage, or loss to persons or property that may result from the use of any ideas, methods, instructions, or products mentioned in the content. Readers are encouraged to independently verify any information before relying on it, and the publisher assumes no responsibility for any consequences arising from the use of materials contained in this publication.

Supplementary Materials

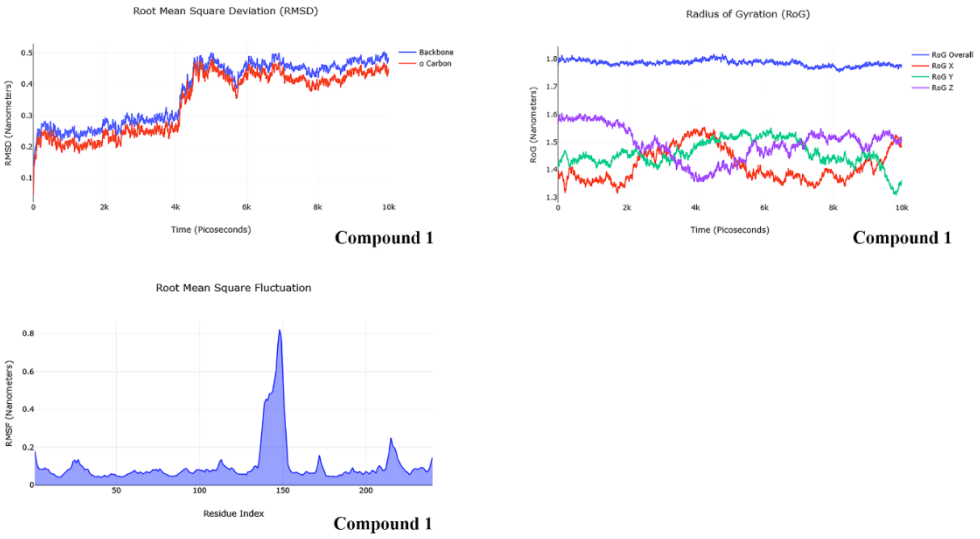

Figure S1. Molecular dynamics simulation of Compound 1.

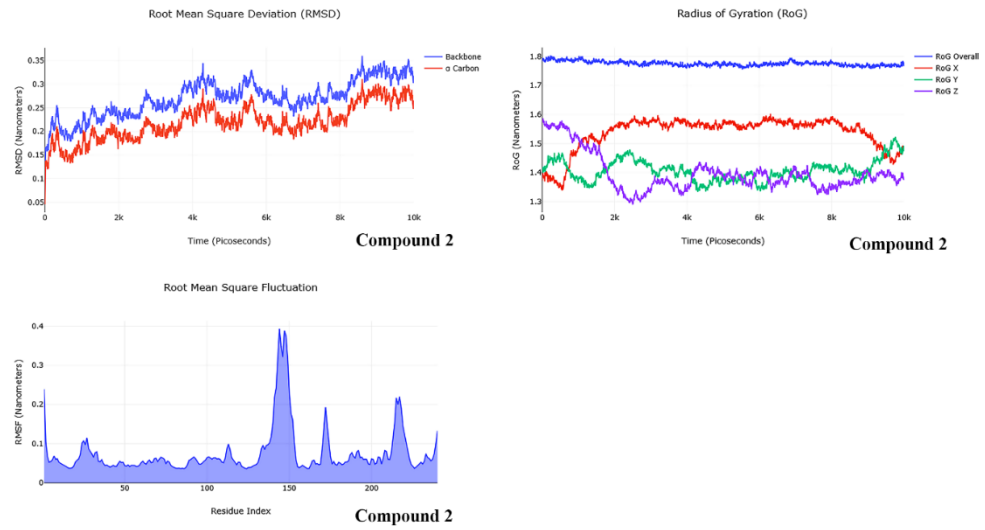

Figure S2. Molecular dynamics simulation of Compound 2.

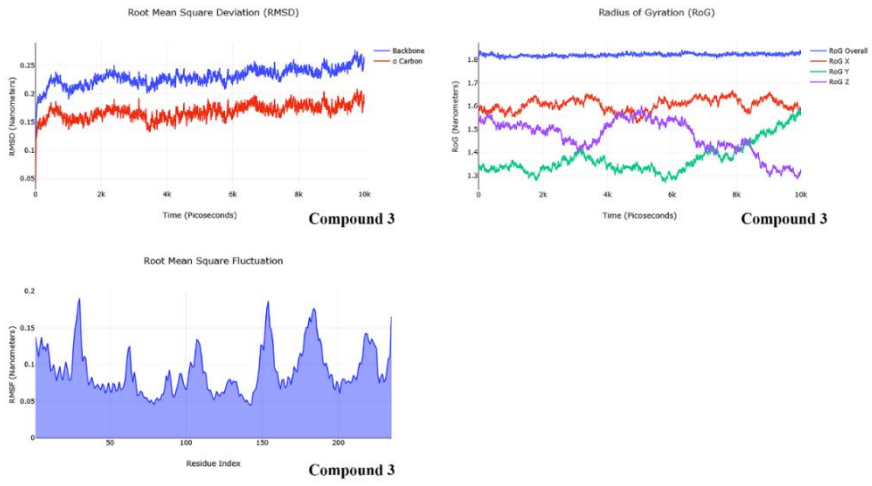

Figure S3. Molecular dynamics simulation of Compound 3.

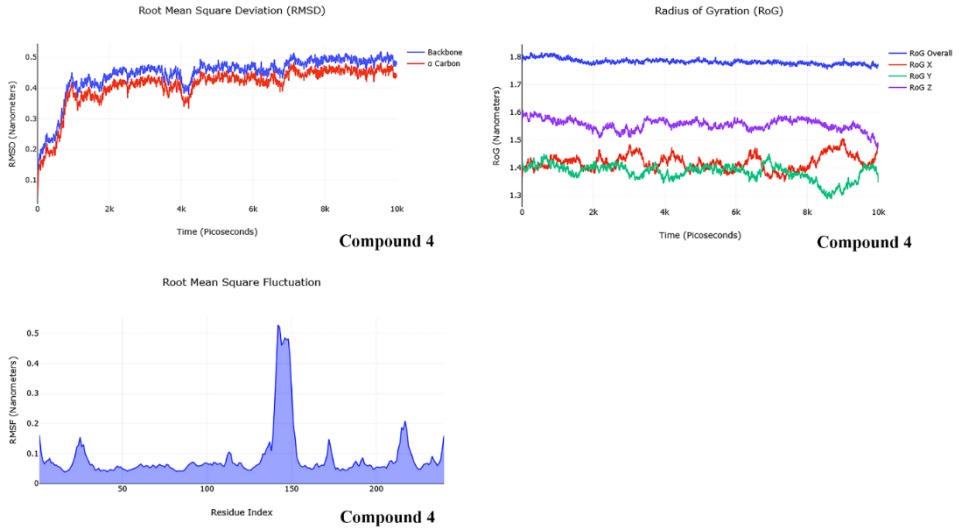

Figure S4. Molecular dynamics simulation of Compound 4.

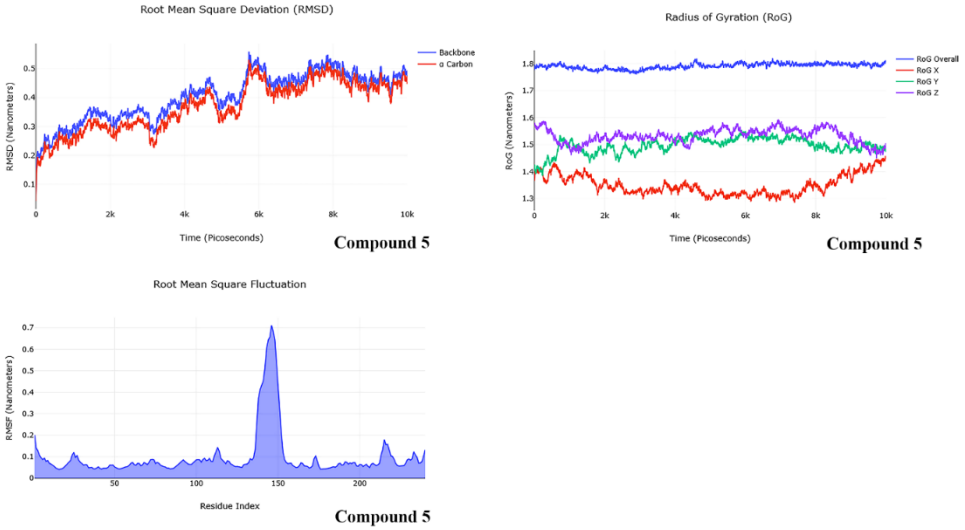

Figure S5. Molecular dynamics simulation of Compound 5.

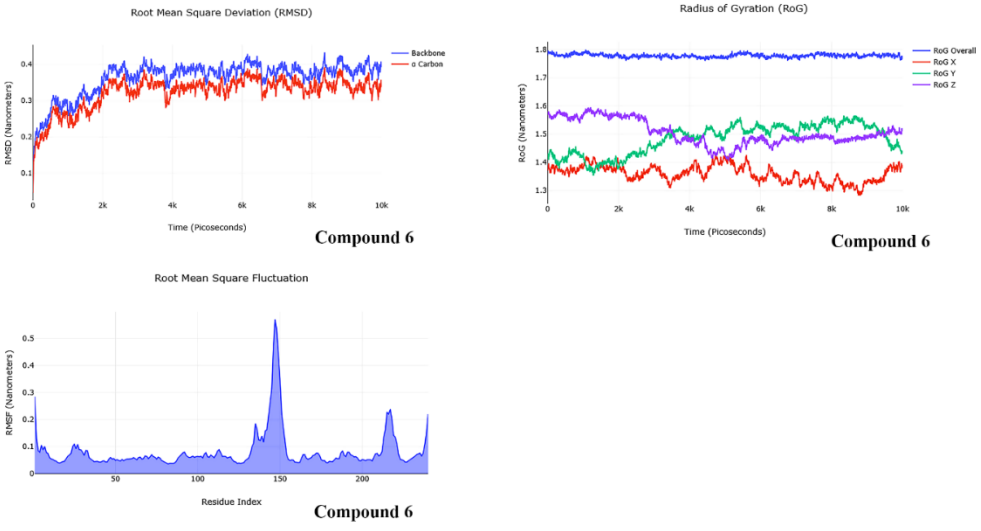

Figure S6. Molecular dynamics simulation of Compound 6.